Reflectionless grating couplers for Silicon-on-Insulator photonic integrated circuits

D. Vermeulen,[1,2,*] **Y. De Koninck,**[1] **Y. Li,**[1] **E. Lambert,**[1] **W. Bogaerts,**[1] **R. Baets,**[1] **and G. Roelkens**[1]

[1] *Photonics Research Group, Department of Information Technology,*
Ghent University - imec, B-9000 Ghent, Belgium
[2] *Acacia Communications, Inc., 3 Clock Tower Place, Suite 210, Maynard, MA 01754, USA*

[*]*Diedrik.Vermeulen@acacia-inc.com*

Abstract: We propose a novel grating coupler design which is inherently reflectionless by focusing the reflected light away from the entrance waveguide. The design rules for this reflectionless grating coupler are explained and the grating coupler design is investigated by means of 3D FDTD simulations for the case of a Silicon-on-Insulator based platform.

© 2012 Optical Society of America

OCIS codes: (130.0130) Integrated optics; (050.0050) Diffraction and gratings.

References and links

1. D. Taillaert, W. Bogaerts, P. Bienstman, T. F. Krauss, P. Van Daele, I. Moerman, S. Verstuyft, K. De Mesel, and R. Baets. "An out-of-plane grating coupler for efficient butt-coupling between compact planar waveguides and single-mode fibers," IEEE J. Quantum Electron. **38**(7):949–955, 2002.
2. D. Vermeulen, S. Selvaraja, P. Verheyen, G. Lepage, W. Bogaerts, P. Absil, D. Van Thourhout, and G. Roelkens. "High-efficiency fiber-to-chip grating couplers realized using an advanced CMOS-compatible Silicon-on-Insulator platform," Opt. Express **18**(17):18278–83, 2010.
3. A. Mekis, S. Gloeckner, G. Masini, A. Narasimha, T. Pinguet, S. Sahni, and P. Dobbelaere. "A grating-coupler-enabled CMOS photonics platform," IEEE J. Sel. Topics Quantum Electron. **99**:1–12, 2010.
4. L. Zhou, Z. Y. Li, Y. Zhu, Y. T. Li, Z. C. Fan, W. H. Han, Y. D. Yu, and J. Z. Yu. "A novel highly efficient grating coupler with large filling factor used for optoelectronic integration," Chinese Physics B **19**:124214, 2010.
5. X. Chen and H. K. Tsang. "Polarization-independent grating couplers for Silicon-on-Insulator nanophotonic waveguides," Opt. Lett. **36**(6):796–798, 2011.
6. X. Chen and H. K. Tsang. "Nanoholes grating couplers for coupling Between Silicon-on-Insulator waveguides and optical fibers," IEEE Photon. J. **1**(3):184–190, 2009.
7. C. R. Doerr, L. Chen, Y. K. Chen, and L. L. Buhl. "Wide bandwidth silicon nitride grating coupler," IEEE Photon. Technol. Lett. **22**(19):1461–1463, 2010.
8. C. Alonso-Ramos, A. Ortega-Moñux, I. Molina-Fernández, P. Cheben, L. Zavargo-Peche, and R. Halir. "Efficient fiber-to-chip grating coupler for micrometric SOI rib waveguides," Opt. Express **18**(14):15189, 2010.
9. N. Na, H. Frish, I. Hsieh, O. Harel, R. George, A. Barkai, H. Rong, and Others. "Efficient broadband silicon-on-insulator grating coupler with low backreflection," Opt. Lett. **36**(11):2101–2103, 2011.
10. D. Taillaert, P. Bienstman, and R. Baets. "Compact efficient broadband grating coupler for silicon-on-insulator waveguides," Opt. Lett. **29**(23):2749–51, 2004.
11. F. Van Laere, T. Claes, J. Schrauwen, S. Scheerlinck, W. Bogaerts, D. Taillaert, L. O'Faolain, D. Van Thourhout, R. Baets. "Compact focusing grating couplers for Silicon-on-Insulator integrated circuits," IEEE Photon. Technol. Lett. **19**(23):1919–1921, 2007.
12. A. F. Oskooi, D. Roundy, M. Ibanescu, P. Bermel, J. D. Joannopoulos, and S. G. Johnson. "Meep: A flexible free-software package for electromagnetic simulations by the FDTD method," Comput. Phys. Commun. **181**(3):687–702, 2010.

---

1. Introduction

Photonic integration is considered to be a key technology for future advancements in optical communication technologies. Scaling down the optical building blocks enables complex and ultra-compact photonic circuits at a fraction of the cost of conventional systems consisting out of discrete components. Choosing an appropriate platform for developing this miniaturization technology is guided by functionality, compatibility, performance, yield and cost. Regarding the last two issues, Silicon-on-Insulator (SOI) is by far the leading technology for low-cost and high-volume photonic integration since it can benefit from the processes developed in the mature electronics industry. Although the high refractive index contrast of SOI reduces the footprint of the integrated photonic devices considerably, it becomes more difficult to achieve a high-performance mode-size convertor between a single-mode optical fiber ($100\,\mu\mathrm{m}^2$) and an integrated optical waveguide ($0.1\,\mu\mathrm{m}^2$). A possible solution is a grating coupler which is a periodic structure that couples light out of the chip to free space or to an optical fiber [1]. Fiber-to-chip grating couplers with very high efficiency have been demonstrated [2]. However, as most papers focus on coupling efficiency, polarization dependency, ease of fabrication and bandwidth, a solution for the back reflection of these grating couplers is only recently being investigated. A typical reflection back in the silicon waveguide circuit for a high-efficiency grating coupler is around $-17\,\mathrm{dB}$ [3]. Other reported high back reflections are $-10\,\mathrm{dB}$ [4], [5] and $-8\,\mathrm{dB}$ [6]. These levels of back reflections are unacceptable for integrated circuits which contain integrated lasers and amplifiers. Furthermore, back reflections are highly unwanted in interferometer based designs. Most approaches to reduce the reflection of the grating focus on optimizing the dimensions of the grating profile itself, thereby achieving back reflections of $-22\,\mathrm{dB}$ [7], $-28\,\mathrm{dB}$ [8] and $-27\,\mathrm{dB}$ [9]. In this paper we will introduce a solution for curved grating couplers which decouples the reflection at the grating from the reflection back into the waveguide, by refocusing the reflected light away from the entrance waveguide.

2. Theoretical outline

There are two main sources which contribute to the reflection from a grating coupler back into the entrance waveguide. The most important source is the second order reflection of the grating, which can be relatively broadband for high-index contrast gratings. Typically one eliminates this second order reflection by tilting the optical fiber under a small angle of around $10°$ with respect to the surface normal [10]. The second source of back reflection is due to the Fresnel reflection at the waveguide/grating coupler interface. This reflection is highly dependent on the grating structure itself and is very difficult to eliminate. In the proposed grating coupler design, we will refocus both sources of reflection away from the entrance waveguide thereby extinguishing the reflection almost completely.

In [11] a compact focusing grating coupler is presented which uses a curved grating to focus the coupled light into a single-mode waveguide, achieving an eight-fold length reduction as compared to a standard linear grating and adiabatic taper, without performance penalty. For the reflectionless grating coupler we follow the same design rules. The grating is curved such that a plane wavefront originating from the tilted optical fiber is diffracted to the TE-polarized mode of a broad SOI waveguide, so that the wavefront is curved cylindrically and focusing occurs in the center of curvature of the wavefront. The easiest way to describe this system is to use a polar coordinate system (r, δ) with the origin placed at the exit point of the entrance waveguide, as shown in Fig. 1. The beam will expand in the slab region with an effective refractive index n_s and after a certain length r_0 it will encounter the grating, thereby experiencing a different effective refractive index n_g. As a first approximation we assume that these effective refractive indices n_s and n_g are equal and thus $\alpha = 180°$ (no refraction between slab and grating region).
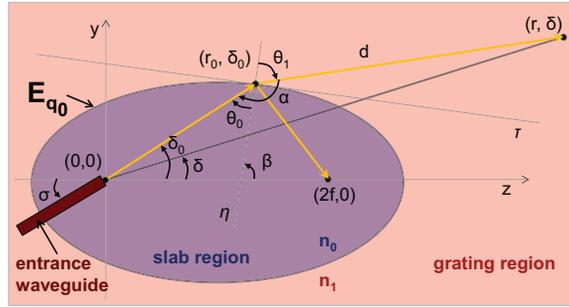
Fig. 1. Focusing grating coupler geometry parameters. The light (yellow arrows) is refracted and reflected at the first grating ellipse E_{q_0}. τ and η are the tangent and normal line respectively of ellipse E_{q0} at point (r_0, δ_0).

The phase matching condition is now [11]:

$$q\lambda_0 = rn_s - rn_c \cos\delta \sin\phi \tag{1}$$

where λ_0 is the vacuum wavelength and q is an integer number corresponding with each grating line. The fiber is tilted under an angle ϕ, the angle between the fiber and the chip surface normal, such that the projected propagation constant of the fiber only has a z-component proportional to $n_c \sin\phi$ where n_c is the refractive index of the top cladding. By rewriting Eq. (1) we can see that the grating lines will form confocal ellipses $E_{q_0}, E_{q_0+1}, ..., E_{q_0+n}$:

$$r = \frac{\frac{q\lambda_0}{n_s}}{1 - \frac{n_c \sin\phi \cos\delta}{n_s}} = \frac{a(1-e^2)}{1 - e\cos\delta} \tag{2}$$

with a common focal point $f_{1,q}$ at the origin. From this we can determine the eccentricity $e = \frac{n_c \sin\phi}{n_s}$, semi-major axis $a = \frac{q\lambda_0 n_s}{n_s^2 - n_c^2 \sin^2\phi}$ and second focal points $f_{2,q} = \frac{q\lambda_0 n_c \sin\phi}{n_s^2 - n_c^2 \sin^2\phi}$. The first grating line corresponds to q_0. The phase matching condition is fulfilled for all parts of the confocal ellipses. We can thus choose which part of the ellipses we use for designing a grating coupler because every part of the ellipse will couple the light out under the same angle ϕ. Normally one takes the right part of the confocal ellipses as shown in Fig. 2(a), such that the propagation vector $\vec{\beta}$ of the entrance waveguide is parallel to the projected wave vector $\vec{k}_z = (2\pi/\lambda)n_c \sin\phi \vec{e}_z$ of the diffracted light (waveguide angle $\sigma = 0°$). Although this seems like the most logical choice, this design will introduce the largest back reflection in the waveguide since the reflection from the grating lines will be refocused to the second focal points $f_{2,q}$ and coupled back into the entrance waveguide. This is solved by using another part of the confocal ellipses as grating coupler and rotating the waveguide by an angle σ of for example $45°$, see Fig. 2(b). In this design the focal points and the grating are not inline hence the grating reflection is focused away from the entrance waveguide into a slab region, thereby fully eliminating the back reflection.

To obtain the appropriate first grating line number q_0, we calculate the in plane aperture opening angle ε of the entrance waveguide using a 3D mode propagation tool. This angle will determine the focusing length of the slab r_0 and thus q_0 such that the width of the diffracted beam matches the width of the Gaussian fiber mode. In [11] it was shown that this focusing length has no influence on the grating coupler performance and can be chosen freely. However, in the reflectionless grating coupler design, the larger the focusing length, the larger is the distance from entrance waveguide to the the closest focal point f_{2,q_0} whereto the reflected light is
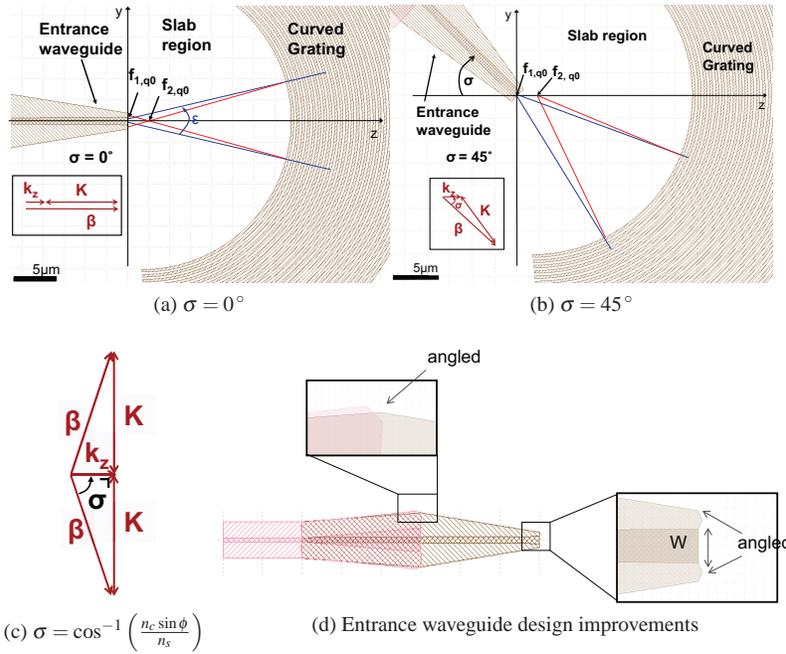
Fig. 2. Reflection from curved grating couplers for different waveguide angles σ. The k-diagram is drawn for $\sigma = 0°$ (a), $\sigma = 45°$ (b) and $\sigma = \cos^{-1}\left(\frac{n_c \sin \phi}{n_s}\right)$ (c) which corresponds to both the optimal reflection waveguide angle and second order reflection angle. ($\vec{K}$ = reciprocal lattice vector) The entrance waveguide is optimized for low reflection (d).

refocused, thereby minimizing the reflection coupled back into the entrance waveguide. On the other hand, a larger focusing length is accompanied by a broader waveguide aperture and thus a larger chance to recapture reflected light back into the entrance waveguide. Depending on the exact entrance waveguide geometry, a proper waveguide width should be chosen.

There exists a waveguide angle σ of the entrance waveguide wherefor the angle between the incident light and the reflected light is maximal. This optimal reflection waveguide angle $\sigma = \cos^{-1}\left(\frac{n_c \sin \phi}{n_s}\right)$ is derived by maximizing the reflection angle $\theta_0(\delta_0)$ given by

$$\theta_0 = \beta - \delta_0 = \frac{\pi}{2} + \tan^{-1}\left(\frac{n_c \sin \phi}{n_s \sin \delta_0} - \cot \delta_0\right) - \delta_0 \tag{3}$$

Figure 3(a) shows θ_0 from Eq. (3) as a function of δ_0 for a fiber angle ϕ of $15°$, wavelength $\lambda_0 = 1.55\,\mu\text{m}$, SiO_2 cladding ($n_c = 1.45$) and $n_s = 2.852$ corresponding to the effective index of the TE slab mode propagating in an SOI slab with a 220nm thick Si core surrounded by SiO_2. The optimal entrance waveguide angle $\sigma = \delta_{0,max}$ for these parameters is $82.4°$ and $68.9°$ for a fiber angle ϕ of $15°$ and $45°$ respectively. In Fig. 3(b) the optimal reflection waveguide angle and the corresponding reflection angle θ_0 are plotted as a function of the fiber tilt angle ϕ. We can conclude that a larger fiber tilt results in a larger reflection angle θ_0 and thus accordingly lower back reflection. A larger fiber tilt will also reduce the second order back reflection (case $\sigma = 0°$) from the grating. However, for practical reasons one typically chooses a tilt angle ϕ between $5°$ and $20°$.
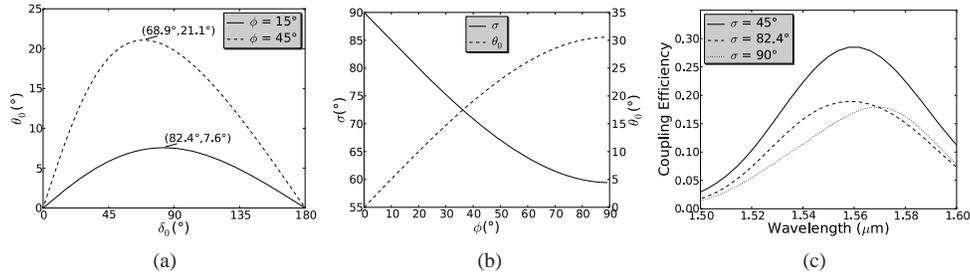
Fig. 3. The reflection angle θ_0 as a function of δ_0 for $\phi = 15^\circ$ (a) and the optimal entrance waveguide angle σ and corresponding θ_0 as a function of ϕ (b) for $\lambda_0 = 1.55\,\mu$m. Simulated coupling efficiency (c) for different waveguide angles σ (etch of 70 nm, $\phi = 15^\circ$).
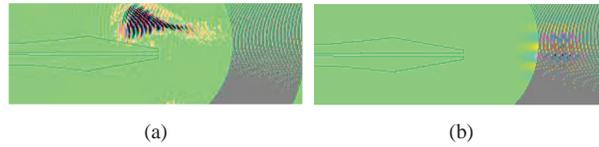

Fig. 4. 3D FDTD simulations showing (a) the refocusing of the reflection using an over-saturated electrical field (Media 1) and (b) waveguide coupling when excited from the fiber (Media 2) ($\sigma = 90^\circ$, $\phi = 15^\circ$)

3. Design improvements

Achieving ultra-low reflections means reducing every possible reflection source. One important source of parasitic reflections is due to discontinuities such as at the exit of the entrance waveguide. These can be minimized by angling the trenches as is shown in Fig. 2(d). The grating reflected and refocused light can be reflected back onto the grating and thus back into the waveguide. Therefore we also need to make sure that the reflected light is not normally incident on any feature.

Another improvement is to differentiate between the effective refractive index of the grating n_g and the effective refractive index of the slab region n_s (see Fig. 1). The phase matching condition for the first grating line corresponding to q_0 will stay the same, i.e. Eq. (1). At this first grating line, the light will transition from a slab with refractive index n_s to a grating region with refractive index n_g and thus be refracted at this interface under an angle $\theta_1 = \sin^{-1}\left(\frac{n_s \sin\theta_0}{n_g}\right)$ according to Snell's law. The angle between the incoming beam and refracted beam is thus $\alpha = \pi + \theta_0 - \theta_1$. Solving the phase condition numerically

$$q\lambda_0 = r_0 n_s + d n_g - r\cos\delta n_c \sin\phi \tag{4}$$

together with the system of geometric equations $d^2 = r_0^2 + r^2 - 2r_0 r\cos(\delta_0 - \delta)$ and $r^2 = r_0^2 + d^2 - 2r_0 d\cos\alpha$ for every refraction point (r_0, δ_0) to (r, δ) will result in the subsequent grating lines for $q \geq q_0 + 1$.

4. 3D FDTD simulations

The grating couplers, designed using Eq. (4), were simulated using full-vectorial 3D FDTD software such as [12]. To calculate the reflection spectra, a pulse with a Gaussian time pro-
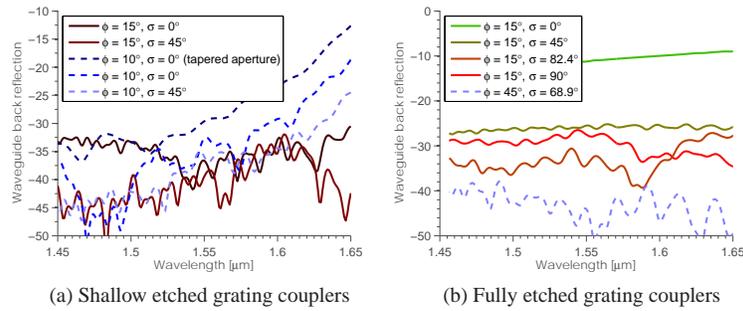
(a) Shallow etched grating couplers   (b) Fully etched grating couplers

Fig. 5. Reflection spectra for shallow (a) and fully etched (b) grating couplers, each time for different values of the waveguide angle σ and fiber tilt angle ϕ.

file was launched in the single-mode access waveguide and the reflected flux was measured in that same waveguide (see Fig. 4(a) (Media 1)). The coupling efficiency was simulated by the normalized power in the single-mode waveguide after launching a Gaussian mode under the correct angles and polarization (see Fig. 4(b) (Media 2)). We have found that the optimal reflection waveguide angle does indeed have the lowest back reflection, but at the price of a coupling efficiency penalty of around 2 dB (see Fig. 3(c)). This is because this waveguide angle corresponds to the angle for second order Bragg reflection (case $\sigma = \cos^{-1}(n_c \sin \phi / n_s)$) when $\vec{K}.\vec{k}_z = 0$ (see Fig. 2(c)). Figure 5 shows the spectra of the reflection back in the entrance waveguide of the proposed grating coupler for different waveguide angles σ. For the shallow etched gratings (70 nm etch in a 220 nm Si core) and for fiber tilt angle $\phi = 10°$, the second order back reflection present at the higher wavelengths decreases by 5 dB to 10 dB for waveguide angles up to $45°$ without coupling efficiency penalty (typical grating coupler efficiency is around 30%) achieving a back reflection of -40 dB (Fig. 5(a)). We see that mainly the second order reflection (case $\sigma = 0°$) present at the higher wavelengths is reduced. This second order reflection can be easily reduced by increasing the fiber tilt angle to $15°$ and even more using the novel grating coupler design. The reflection reduction is the most pronounced in the case of fully etched grating couplers (220 nm etch in a 220 nm Si core) having a typical efficiency around 10%. The back reflection decreases from -7 dB to -28 dB for $\sigma = 45°$ (Fig. 5(b)).

5. Conclusion

We have investigated a reflectionless grating coupler design by means of 3D FDTD simulations. The grating is curved and refocuses the reflection away from the entrance waveguide thereby realizing a 5 dB to 10 dB reflection reduction down to -40 dB for shallow etched gratings, the same back reflection performance of a typical optical fiber connector, without introducing a coupling efficiency penalty. Furthermore, we showed that this method can be used to reduce the reflection of highly reflective (-7 dB) deeply etched grating couplers to useful reflections of -28 dB. These devices could become key components in interferometer based designs and circuits using integrated lasers and amplifiers.

Acknowledgements